Flat-band optical phonons in twisted bilayer graphene

Emmanuele Cappelluti,[1] Jose Angel Silva-Guillén,[2,*] Habib Rostami,[3,4] and Francisco Guinea[2,5,†]
[1]*Istituto di Struttura della Materia, CNR (ISM-CNR), 34149 Trieste, Italy*
[2]*Instituto Madrileño de Estudios Avanzados, IMDEA Nanociencia, Calle Faraday 9, 28049 Madrid, Spain*
[3]*Department of Physics, University of Bath, Claverton Down, Bath BA2 7AY, United Kingdom*
[4]*Nordita, KTH Royal Institute of Technology and Stockholm University, Hannes Alfvéns väg 12, 10691 Stockholm, Sweden*
[5]*Donostia International Physics Center, Paseo Manuel de Lardizábal 4, 20018 San Sebastián, Spain and Ikerbasque, Basque Foundation for Science, 48009 Bilbao, Spain*

(Received 19 March 2023; accepted 17 August 2023; published 1 September 2023)

Twisting bilayer sheets of graphene have been proven to be an efficient way to manipulate the electronic Dirac-like properties, resulting in flat bands at magic angles. Inspired by the electronic model, we develop a continuum model for the lattice dynamics of twisted bilayer graphene and we show that a remarkable band flattening applies to almost all the high-frequency in-plane lattice vibration modes, including the valley Dirac phonon, valley optical phonon, and zone-center optical phonon bands. Utilizing an approximate approach, we estimate small but finite magic angles at which a vanishing phonon bandwidth is expected. In contrast to the electronic case, the existence of a restoring potential prohibits the emergence of a magic angle in a more accurate modeling. The predicted phonon band flattening is highly tunable by the twist angle and this strong dependence is directly accessible by spectroscopic tools.

DOI: 10.1103/PhysRevB.108.125401

I. INTRODUCTION

The exotic electronic, optical, and lattice properties of graphene have been enriched in the past few years by the additional possibility of manipulating two graphene layers with a finite twist angle. In twisted bilayer graphene (TBG), a complex phase diagram, including superconductivity, a Mott insulating phase, and a novel topology of the electronic bands have been revealed [1–4]. A key ingredient in this scenario is the existence of a nontrivial electronic structure with very narrow bandwidth, also known as flat bands, at the so-called magic angle [5–7] has been analyzed using schemes based on either tight-binding models [5,6] or continuum models [8–10].

Nevertheless, along with the investigation focused on the electronic properties, a large interest has also recently arisen concerning the effects of twist on the lattice dynamics. The phonon spectrum in TBG has been studied theoretically [11] and experimentally [12]. Optical [13,14] and acoustical [15,16] phonons have been investigated as possible origins of the observed superconductivity. A particular high-energy optical mode at the K and K' points has been extensively studied in TBG [17–19], as it gives rise to flat moiré bands and it couples strongly to electrons. Further evidence of a crucial role of the K-point optical phonons in the superconducting pairing has been provided in Refs. [20,21]. These modes are also currently thought to be responsible for the remarkable features in Raman spectroscopy of single-layer and multilayer graphene [22–26]. Concerning the possibility of a strong twist-driven renormalization of the phonon dispersion, calculations based on models of elastic systems have also been carried out. In Ref. [27], the emergence of a flat band associated with out-of-plane flexural modes was shown. Similar results for the out-of-plane lattice modes were predicted for twisted "artificial" graphene systems [28]. In-plane lattice modes at the K and K' points, also characterized by Dirac physics, appear as well, however, and are even more interesting. On the one hand, these modes were initially associated with the onset of the D and 2D Raman features [29,30]. On the other hand, the same modes, in the presence of a symmetry breaking of the sublattices as in h-BN or in transition-metal dichalcogenides (TMDs), can host chiral content that enforces fundamental selection rules [31–35]. In this scenario, it is worth mentioning that flat bands have also been predicted in moiré structures of twisted two-dimensional TMDs [36,37].

In this paper, we investigate the effect of twist on the main high-energy (optical) modes at the high-symmetry points Γ and K of the phonon spectrum of TBG, with a special focus on the Dirac-like in-plane lattice modes at K. Using a force-constant (FC) model and a proper generalization of the continuum approach for the lattice phonon modes, we show that (i) in-plane Dirac phonons, upon twist, undergo a strong renormalization of the effective dispersion giving rise to flat bands, in a similar way as Dirac-like electrons do; (ii) a "magic" angle, where the dispersion of these modes approaches zero, can be analytically predicted, and numerically observed, at twist angles remarkably larger than the ones required for the existence of flat bands in the electronic spectrum. Furthermore, we show that the appearance of flat bands is also predicted (at smaller twist angles) for the high-frequency transverse-optical (TO) phonon at K and for

*josilgui@gmail.com
†paco.guinea@gmail.com

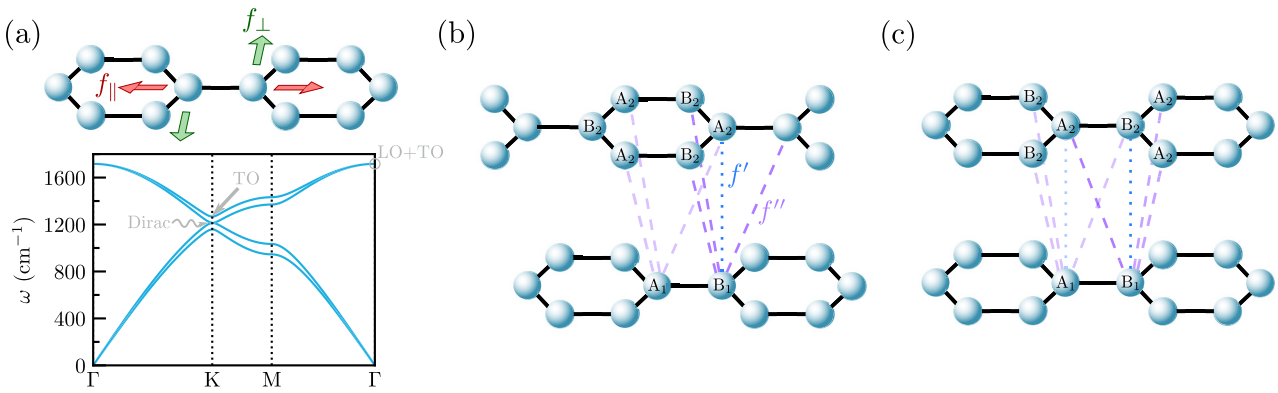

FIG. 1. Force-constant model for the untwisted cases. (a) Single-layer graphene (top) and its phonon dispersion calculated using the model. Only the elastic coupling f (solid black lines) between nearest-neighbor atoms f is retained. The colored arrows denote the lattice displacements coupled with the two elastic components, $f_\parallel$ (red) and $f_\perp$ (green). (b), (c) *AB* and *AA* bilayer graphene, respectively. The two further interlayer elastic couplings are shown, f' (dotted blue lines) and f'' (dashed purple lines).

the longitudinal-optical/transverse-optical (LO/TO) modes at the Γ point, thus rationalizing the numerical results of Ref. [17]. Finally, note that our analysis does not include the low-angle regime, where lattice relaxation leads to *AB* and *BA* domains separated by boundaries, and the low-energy phonons are determined by fluctuations of these boundaries [38–43].

II. THE MODEL

A suitable continuum model for the lattice dynamics of TBG is derived from a FC model. Following the well-known scheme [7–9], we first construct the proper Hamiltonian for the single layer, and for the representative limit cases of *AA* and *AB* bilayer stacking. The lattice dynamics for the twisted system is further obtained by including the appropriate tunneling between a $\mathbf{q}$ vector in one layer with a $\mathbf{q}+\mathbf{Q}_\nu$ vector in the other layer, where $\mathbf{Q}_\nu$ are the characteristic tunneling momenta, just as for the electronic case. In order to focus on the physics of the Dirac phonons, we restrict our model to in-plane lattice displacements responsible for the Dirac modes, defining an eightfold Hilbert basis, $u_{\alpha,i}(\mathbf{q})$, corresponding to the lattice displacements of the four atoms in the $x-y$ space [44]. Here, $i=x,y$ are the Cartesian indices and $\alpha = A_1, B_1, A_2, B_2$ labels the atoms in the sublattice A, B in layer 1, 2.

The phonon band structure is thus obtained by the solution of the secular equation,

$$M\,\hat{\omega}^2(\mathbf{q})\cdot\mathbf{u}(\mathbf{q}) = \hat{\mathbf{K}}(\mathbf{q})\cdot\mathbf{u}(\mathbf{q}), \tag{1}$$

where M is the carbon mass, $\hat{\omega}^2(\mathbf{q})$ the diagonal matrix of the square frequencies, and $\hat{\mathbf{K}}(\mathbf{q})$ the dynamical matrix that takes into account the elastic couplings between different carbon atoms. In order to provide the clearest analytical insight into the manipulation of the Dirac lattice modes, we include the minimum set of FC parameters preserving the relevant physics. More explicitly, in a single layer, we include elastic coupling only between in-plane nearest-neighbor atoms, described by two parameters, $f_\parallel$, and $f_\perp$, ruling the relative radial and in-plane tangential lattice displacements between neighbor atoms at interatomic distance a [see Fig. 1(a)]. The coupling between different layers in the *AA* and *AB* structures is thus described by two more kinds of elastic forces [see Figs. 1(b) and 1(c)]: $f'_\perp$ vertically connecting two atoms atop each other at the distance c; and f'' connecting atoms in different layers at distance $R=\sqrt{a^2+c^2}$, with the relevant components $f''_\parallel$ and $f''_\perp$, governing, respectively, the relative in-plane longitudinal and transverse displacement of two atoms with respect to their joining vector. The resulting dynamical matrix can thus be written as

$$\hat{\mathbf{K}}(\mathbf{q}) = \hat{\mathbf{K}}^{f}(\mathbf{q}) + \hat{\mathbf{K}}^{f'}(\mathbf{q}) + \hat{\mathbf{K}}^{f''}(\mathbf{q}). \tag{2}$$

III. DIRAC PHONONS AT *K*

The Dirac phonons at the K point are more conveniently described by introducing a chiral basis $\tilde{u}_{\alpha,\nu}(\mathbf{q})$, where $\nu = R, L$ and $\tilde{u}_{\alpha,\mathrm{R/L}} = (u_{\alpha,x} \pm i u_{\alpha,y})/\sqrt{2}$. The dynamical matrices for the *AA* and *AB* structures in this basis read

$$\hat{\mathbf{K}}^{f}(\mathbf{q}) = \sum_\nu \hat{f}_\nu \hat{\sigma}_0[\hat{\tau}_0 - \pi'_\nu(\mathbf{q})\hat{\tau}_x + \pi''_\nu(\mathbf{q})\hat{\tau}_y], \tag{3}$$

$$\hat{\mathbf{K}}^{f'}_{\mathrm{AA}}(\mathbf{q}) = \hat{f}'_\perp[\hat{\sigma}_0 + \hat{\sigma}_x]\hat{\tau}_0, \tag{4}$$

$$\hat{\mathbf{K}}^{f'}_{\mathrm{AB}}(\mathbf{q}) = \hat{f}'_\perp[\hat{\sigma}_0\hat{\tau}_0 - \hat{\sigma}_z\hat{\tau}_z + \hat{\sigma}_x\hat{\tau}_x + \hat{\sigma}_y\hat{\tau}_y]/2, \tag{5}$$

$$\hat{\mathbf{K}}^{f''}_{\mathrm{AA}}(\mathbf{q}) = \sum_\nu \hat{f}''_\nu[\hat{\sigma}_0\hat{\tau}_0 - \pi'_\nu(\mathbf{q})\hat{\sigma}_x\hat{\tau}_x + i\pi''_\nu(\mathbf{q})\hat{\sigma}_y\hat{\tau}_y], \tag{6}$$

$$\begin{aligned}\hat{\mathbf{K}}^{f''}_{\mathrm{AB}}(\mathbf{q}) = \sum_\nu \hat{f}''_\nu\{&[3\hat{\sigma}_0\hat{\tau}_0 - \hat{\sigma}_z\hat{\tau}_z]/2 \\ &- \sum_\nu \hat{f}''_\nu\pi'_\nu(\mathbf{q})[\hat{\sigma}_x\hat{\tau}_0 - (\hat{\sigma}_x\hat{\tau}_x - \hat{\sigma}_x\hat{\tau}_x)/2] \\ &+ \sum_\nu \hat{f}''_\nu\pi''_\nu(\mathbf{q})[i\hat{\sigma}_y\hat{\tau}_0 - (\hat{\sigma}_x\hat{\tau}_y + \hat{\sigma}_y\hat{\tau}_x)/2]\},\end{aligned} \tag{7}$$

where $\hat{\tau}_i$ are Pauli matrices acting in the (A,B) sublattice space, $\hat{\sigma}_i$ are Pauli matrices acting in the layer space, and $\hat{f}_\nu$, $\hat{f}'_\nu$, $\hat{f}''_\nu$ are 2×2 matrices defined in the (R,L) chiral space, whose explicit expressions are reported in the Supplemental Material (SM) [45]. The index ν runs over the three vectors

of the in-plane nearest-neighbor B atoms with respect to an atom A, also determining the effective phonon dispersion by the nonlocal factors $\pi'_\nu(\mathbf{q}) = \mathrm{Re}\{\exp[i\mathbf{q}\cdot\boldsymbol{\delta}_\nu]\}$, $\pi''_\nu(\mathbf{q}) = \mathrm{Im}\{\exp[i\mathbf{q}\cdot\boldsymbol{\delta}_\nu]\}$, $\boldsymbol{\delta}_1 = (1,0)$, $\boldsymbol{\delta}_2 = (-1/2, \sqrt{3}/2)$, and $\boldsymbol{\delta}_3 = (-1/2, -\sqrt{3}/2)$. Note that the term $\hat{\mathbf{K}}^f(\mathbf{q})$ in the dynamical matrix does not depend on the specific AA or AB (or twisted) structure since it is purely related to intralayer physics.

Without interlayer coupling, the phonon dispersion exhibits two degenerate Dirac cones at the K point, emerging from the longitudinal-acoustic (LA) and longitudinal-optical (LO) branches for each layer. In an AA structure, these cones split into two, while only one survives in AB stacking and the other one is gapped due to the interlayer coupling. To determine the intralayer FC parameters $f_\parallel$ and $f_\perp$, we fix the energy of the single-layer Dirac point $\omega_0 = \sqrt{3(f_\parallel + f_\perp)/2M}$ and their Dirac velocity $v = \omega_0 a(f_\parallel - f_\perp)/4(f_\parallel + f_\perp)$. The other three interlayer elastic parameters $f'_\perp$, $f''_\parallel$, $f''_\perp$ can be determined by fixing the energies of the two Dirac cones in the AA structure, $\omega_{\mathrm{AA},\pm}$ [46], and by the splitting energy of the single-degenerate levels in the AB stacking, $\omega_{\mathrm{AB},\pm}$ [45]. Using first-principles calculations (see the Supplemental Material (SM) [45] and the references therein [47–53]), we obtain $f_\parallel = 23.882$, $f_\perp = 19.973$, $f'_\perp = -0.143$, $f''_\parallel = 0.090$, and $f''_\perp = 0.059\mathrm{meV/AA}^2$.

Utilizing the dynamical matrix of two uncoupled layers and that of the AA and AB structures, we construct a continuum model in the twisted case. Here we investigate the effects of twist on the properties of a few selected in-plane lattice modes, namely, the Dirac phonons at the K point emerging from the LA and LO branches, and the nondegenerate high-frequency TO mode at the K point. Furthermore, we study the degenerate LO and TO modes at the Γ point. For Dirac phonons, we restrict the analysis to the relevant fourfold Hilbert subspace containing the left-hand chiral displacements for the $A1/A2$ atoms, and the right-hand chiral displacements for the $B1/B2$ atoms. The 4×4 dynamical matrices so obtained read

$$\hat{\mathcal{K}}_{\mathrm{AA}}(\tilde{\mathbf{q}}) = v\hat{\sigma}_0[\tilde{q}_x\hat{\tau}_x + \tilde{q}_y\hat{\tau}_y] + V_{\mathrm{AA}}\hat{\sigma}_0\hat{\tau}_0 - f'_\perp\hat{\sigma}_x\hat{\tau}_0, \quad (8)$$

$$\hat{\mathcal{K}}_{\mathrm{AB}}(\tilde{\mathbf{q}}) = v\hat{\sigma}_0[\tilde{q}_x\hat{\tau}_x + \tilde{q}_y\hat{\tau}_y] + V_{\mathrm{AB},0}\hat{\sigma}_0\hat{\tau}_0 + V_{\mathrm{AB},z}\hat{\sigma}_z\hat{\tau}_z - 3(f''_\parallel - f''_\perp)/4[\hat{\sigma}_x\hat{\tau}_x + \hat{\sigma}_y\hat{\tau}_y], \quad (9)$$

where $\tilde{q}_i$ are wave vectors measured with respect to the K point and where the parameters V_{AA}, $V_{\mathrm{AB},0}$, and $V_{\mathrm{AB},z}$ are ruled by the interlayer force constants (for an explicit expression, see the SM [45]).

Equations (8) and (9) provide the basis for assessing the evolution of the Dirac phonons in TBG within a continuum model. Following a similar approach as for electrons, we describe the dynamical matrix for a twisted bilayer by interpolating the off-diagonal blocks of the AA and AB matrices in Eqs. (8) and (9) [8]. We find that the equivalent of an AA and AB interlayer tunneling is ruled by the following terms:

$$t_{\mathrm{AA}} = -f'_\perp/3, \quad (10)$$

$$t_{\mathrm{AB}} = -(f''_\parallel - f''_\perp)/2. \quad (11)$$

Furthermore, we notice that the diagonal elements of Eqs. (8) and (9) give rise to effective local potentials which are different for different local stackings, and hence in different regions in real space corresponding to an AA, AB, or BA stacking [45]. These potentials can be expanded in reciprocal lattice vectors similarly to the way electrostatic potentials are incorporated into the continuum model for electronic bands of TBG [54]. Including these local potentials in this scheme, we show, in Figs. 2(a) and 2(b), the evolution with the twist angle of the phonon dispersion close to the in-plane Dirac energies in the moiré Brillouin zone. We can notice an overall upward energy shift of all the phonon frequencies, stemming from the presence of such local potentials. Moreover, the phonon dispersion still shows a dispersive Dirac behavior close to K for $\theta = 4^\circ$, with a linear dispersion velocity comparable with the single layer. Interestingly, such dispersion appears much flatter at $\theta = 1.05^\circ$, signalizing a remarkable band renormalization. In order to get a qualitative estimate of a possible "phonon magic angle," we can employ the standard approach of truncating the interlayer tunneling only to the first set of three momenta $\mathbf{Q}_\nu$ [7] and we get $\bar{\theta}_{\mathrm{LO/LA}} \approx 2.1^\circ$ (see SM [45]). Such a picture is supported by a quantitative analysis based on multi-interlayer scattering, including local potentials. Within this framework, following Ref. [7], the flattening of the LO/LA phonon bands can be parameterized in terms of the renormalization factor $R = V^*/V$ of the Dirac phonon velocity V^* in the twisted case with respect to the one in the single layer, V. The twist-angle dependence of R for the full multiscattering continuum model is plotted in Fig. 2(c), showing a marked depletion for twist angles $\lesssim 2^\circ$. Nevertheless, such depletion, for these as for other lattice modes, never reaches a perfect flattening because of the role of the local potentials; the qualitative estimate of the phonon magic angle can properly capture the correct range of twist angles where a strong phonon band renormalization occurs.

IV. TO PHONON AT K

The analysis done for Dirac phonons at K can be also extended to the TO phonon at K, which induces intervalley scattering for the electrons [17]. Following the usual scheme, the phonon wave function is expanded in plane waves in the two layers, where the plane wave in one layer is transferred as a superposition of three plane waves in the neighboring layer (see SM [45] for more details). The main differences with respect to the LO/LA modes are the following: (i) The monolayer TO phonon is not degenerate at K, so that the spinor (sublattice) degree of freedom disappears. (ii) The dispersion in the monolayer is quadratic in $\tilde{\mathbf{q}}$. The coupling between layers includes a diagonal restoring term, which changes from the AA to the AB and BA regions, and a single interlayer coupling, which also depends on the position within the unit cell. This coupling is finite in the AA region, and it vanishes in the AB and BA regions [45]. Hence, the model includes four parameters, which can be readily obtained from the FCs discussed above. The model used here resembles those used for the conduction band edge of MoS_2 (located at the K and K' points) [55,56]. The representative plots of the TO phonon dispersion in the moiré Brillouin zone are shown in Figs. 2(d) and 2(e), and the angle dependence of the appropriate band renormalization for the TO modes is depicted in Fig. 2(f). Using the standard approximate model restricted to the first star

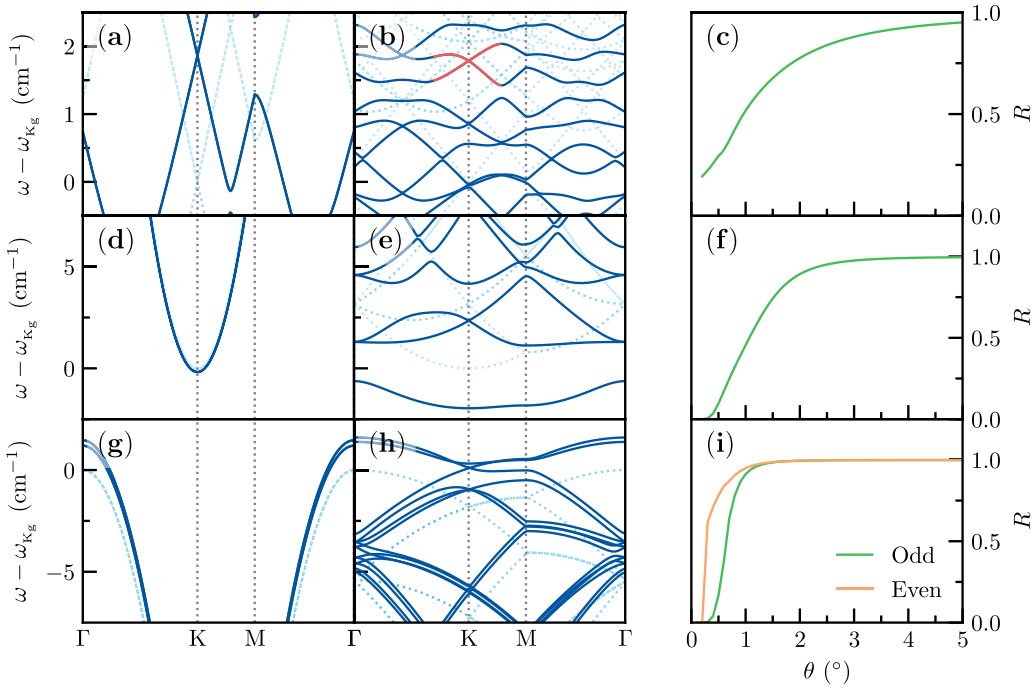

FIG. 2. Evolution with the twist angle of the phonon dispersion in the moiré Brillouin zone for the LO/LA modes at K (top panels), the TO mode at K (middle panels), and the TO modes at Γ (bottom panels). Left panels are for twist angle $\theta = 4^\circ$; central panels are for $\theta = 1.05^\circ$. Dark-blue solid and light-blue dotted lines represent the results with and without interlayer coupling, respectively. In panel (b), the relevant Dirac modes in the twisted cases are highlighted in red. In the right panels, we show the band renormalization factor R for each mode as a function of twist angle.

of Bloch waves and neglecting the diagonal restoring forces, we can also obtain, for these modes, an estimate for the magic angle at which the prefactor of the quadratic dispersion at K vanishes [45]. We obtain $\bar{\theta}_{TO} \approx 1.0^\circ$, which is qualitatively consistent with the results shown in Fig. 2(f).

V. OPTICAL PHONONS AT Γ

The continuum model for the optical phonons at Γ in TBG is particularly simplified by the fact that each plane wave in one layer just tunnels into a single plane wave in the other layer. As detailed in the SM [45], the interlayer forces thus separately couple the LO and the TO modes. One can further divide modes with even and odd symmetry with respect to the vertical axis. The LO and TO modes of the single layer thus evolve in TBG into four *independent* bands with a quadratic dispersion which is ruled by different combinations of the FC parameters, and hence with four different behaviors for the band renormalization [45]. The model resembles electronic models used for the valence band edge of MoS_2 (located at the Γ point) [57–59]. The plots of the phonon dispersion of the TO modes with even and odd symmetry for different twist angles are shown in Figs. 2(g) and 2(h), and the angle dependence of the effective band renormalization in Fig. 2(i). Similar results (not shown) are obtained for the LO modes.

VI. DISCUSSION

We have analyzed the optical phonons of TBG, by introducing proper continuum models originally devised for the electronic structure. For all three cases studied, i.e., LO/LA modes at K, TO modes at K, and LO/TO modes at Γ, we find a remarkable flattening of the superlattice phonon bands at low twist angles, starting at higher values than the "magic angles" where electronic flat bands appear. The possibility of inducing flat optical-phonon bands in a twist range different from the magic angle for electronic bands can have interesting consequences on the role of these modes in the superconducting pairing, opening the possibility of controlling independently flat bands in the electronic and lattice degrees of freedom. In this regard, it is interesting to notice the recent observation of remarkable replicas of the electron bands with a well-defined energy spacing, $\omega_0 \sim 150$ meV [20,21]. Such replicas have been ascribed to a strong electron-phonon coupling with the TO modes at K, whereas the evidence of replicas with a well-defined energy ω_0 supports a scenario with a dispersionless Einstein mode. The onset of flat phonon bands is also expected to tune the optical properties of TBG in the infrared frequency range, providing a possible tool for twist characterization. LO/TO modes are directly probed by one-phonon Raman and infrared spectroscopy in bilayer graphene [60], with intensities and selection rules that crucially depend on the bilayer stacking order and on the z-axis symmetry [61–65], and hence on twisting [66–69]. The sensitivity to gate-induced symmetry breaking can also provide a further tool for characterizing different flat branches' [70] TO modes, and their dispersions close to the K point are also commonly observed by means of double-resonance processes D and 2D [22–26]. Finally, although a direct contribution of the LO/LA modes at K to the Raman phonon spectroscopy is not well assessed [22,24,29,30], these modes bear a promising relevance for quantum devices since, obeying a similar Dirac

quantum structure, they are expected to show a similar rich complexity as the electronic degree of freedom. It is also worth mentioning that the same modes in the presence of mass disproportion (e.g., in h-BN) host chiral phonon states supporting a finite lattice angular momentum [31–34], with possible application towards suitable (lattice-based) quantum two-level systems [36,37].

ACKNOWLEDGMENTS

The authors thank T. Cea and H. Ochoa for useful discussions. IMDEA Nanociencia acknowledges support from the "Severo Ochoa" Programme for Centres of Excellence in R&D (Grant No. CEX2020-001039-S/AEI/10.13039/501100011033). F.G. acknowledges funding from the European Commission, within the Graphene Flagship, Core 3, Grant No. 881603, and from Grants No. NMAT2D (Comunidad de Madrid, Spain) and No. SprQuMat (Ministerio de Ciencia e Innovación, Spain), and financial support through the (MAD2D-CM)-MRR MATERIALES AVANZADOS-IMDEA-NC. E.C. acknowledges financial support from PNRR MUR Project No. PE0000023-NQSTI. H.R. acknowledges the support from the Swedish Research Council (VR Starting Grant No. 2018-04252).

[1] Y. Cao, V. Fatemi, S. Fang, K. Watanabe, T. Taniguchi, E. Kaxiras, and P. Jarillo-Herrero, Nature (London) **556**, 43 (2018).
[2] M. Fidrysiak, M. Zegrodnik, and J. Spałek, Phys. Rev. B **98**, 085436 (2018).
[3] Y. Cao, V. Fatemi, A. Demir, S. Fang, S. L. Tomarken, J. Y. Luo, J. D. Sanchez-Yamagishi, K. Watanabe, T. Taniguchi, E. Kaxiras, R. C. Ashoori, and P. Jarillo-Herrero, Nature (London) **556**, 80 (2018).
[4] Y. Saito, J. Ge, K. Watanabe, T. Taniguchi, and A. F. Young, Nat. Phys. **16**, 926 (2020).
[5] E. Suárez Morell, J. D. Correa, P. Vargas, M. Pacheco, and Z. Barticevic, Phys. Rev. B **82**, 121407 (2010).
[6] G. Trambly de Laissardière, D. Mayou, and L. Magaud, Nano Lett. **10**, 804 (2010).
[7] R. Bistritzer and A. H. MacDonald, Proc. Natl. Acad. Sci. **108**, 12233 (2011).
[8] J. M. B. Lopes dos Santos, N. M. R. Peres, and A. H. Castro Neto, Phys. Rev. Lett. **99**, 256802 (2007).
[9] E. J. Mele, Phys. Rev. B **84**, 235439 (2011).
[10] Y. Ren, Q. Gao, A. H. MacDonald, and Q. Niu, Phys. Rev. Lett. **126**, 016404 (2021).
[11] A. I. Cocemasov, D. L. Nika, and A. A. Balandin, Phys. Rev. B **88**, 035428 (2013).
[12] A. Jorio and L. G. Cançado, Solid State Commun. **175–176**, 3 (2013).
[13] F. Wu, A. H. MacDonald, and I. Martin, Phys. Rev. Lett. **121**, 257001 (2018).
[14] Y. W. Choi and H. J. Choi, Phys. Rev. Lett. **127**, 167001 (2021).
[15] B. Lian, Z. Wang, and B. A. Bernevig, Phys. Rev. Lett. **122**, 257002 (2019).
[16] F. Wu, E. Hwang, and S. Das Sarma, Phys. Rev. B **99**, 165112 (2019).
[17] M. Angeli, E. Tosatti, and M. Fabrizio, Phys. Rev. X **9**, 041010 (2019).
[18] M. Angeli and M. Fabrizio, Eur. Phys. J. Plus **135**, 630 (2020).
[19] A. Blason and M. Fabrizio, Phys. Rev. B **106**, 235112 (2022).
[20] C. Chen, K. Nuckolls, S. Ding, W. Miao, D. Wong, M. Oh, R. Lee, S. He, C. Peng, D. Pei, Y. Li, S. Zhang, J. Liu, Z. Liu, C. Jozwiak, A. Bostwick, E. Rotenberg, C. Li, X. Han, D. Pan *et al.*, arXiv:2303.14903.
[21] C.-X. Liu, Y. Chen, A. Yazdani, and B. Bernevig, arXiv:2303.15551.
[22] A. C. Ferrari and J. Robertson, Phys. Rev. B **61**, 14095 (2000).
[23] S. Piscanec, M. Lazzeri, F. Mauri, A. C. Ferrari, and J. Robertson, Phys. Rev. Lett. **93**, 185503 (2004).
[24] A. C. Ferrari, J. C. Meyer, V. Scardaci, C. Casiraghi, M. Lazzeri, F. Mauri, S. Piscanec, D. Jiang, K. S. Novoselov, S. Roth, and A. K. Geim, Phys. Rev. Lett. **97**, 187401 (2006).
[25] D. M. Basko, Phys. Rev. B **76**, 081405 (2007).
[26] D. M. Basko, Phys. Rev. B **78**, 125418 (2008).
[27] M. Rosendo López, F. Peñaranda, J. Christensen, and P. San-Jose, Phys. Rev. Lett. **125**, 214301 (2020).
[28] Y. Deng, M. Oudich, N. J. Gerard, J. Ji, M. Lu, and Y. Jing, Phys. Rev. B **102**, 180304 (2020).
[29] M. J. Matthews, M. A. Pimenta, G. Dresselhaus, M. S. Dresselhaus, and M. Endo, Phys. Rev. B **59**, R6585(R) (1999).
[30] C. Thomsen and S. Reich, Phys. Rev. Lett. **85**, 5214 (2000).
[31] L. Zhang and Q. Niu, Phys. Rev. Lett. **112**, 085503 (2014).
[32] L. Zhang and Q. Niu, Phys. Rev. Lett. **115**, 115502 (2015).
[33] H. Zhu, J. Yi, M.-Y. Li, J. Xiao, L. Zhang, C.-W. Yang, R. A. Kaindl, L.-J. Li, Y. Wang, and X. Zhang, Science **359**, 579 (2018).
[34] H. Chen, W. Zhang, Q. Niu, and L. Zhang, 2D Mater. **6**, 012002 (2019).
[35] H. Rostami, F. Guinea, and E. Cappelluti, Phys. Rev. B **105**, 195431 (2022).
[36] N. Suri, C. Wang, Y. Zhang, and D. Xiao, Nano Lett. **21**, 10026 (2021).
[37] I. Maity, A. A. Mostofi, and J. Lischner, Phys. Rev. B **105**, L041408 (2022).
[38] M. Koshino and Y.-W. Son, Phys. Rev. B **100**, 075416 (2019).
[39] H. Ochoa, Phys. Rev. B **100**, 155426 (2019).
[40] M. Koshino and N. N. T. Nam, Phys. Rev. B **101**, 195425 (2020).
[41] H. Ochoa and R. M. Fernandes, Phys. Rev. Lett. **128**, 065901 (2022).
[42] J. Z. Lu, Z. Zhu, M. Angeli, D. T. Larson, and E. Kaxiras, Phys. Rev. B **106**, 144305 (2022).
[43] L. P. A. Krisna and M. Koshino, Phys. Rev. B **107**, 115301 (2023).
[44] The relevance of a finite mixing between the in-plane and out-of-plane modes is discussed in a devoted section in the

Supplemental Material, supporting the validity of the analysis in the reduced space retaining only in-plane lattice displacements.

[45] See Supplemental Material at http://link.aps.org/supplemental/10.1103/PhysRevB.108.125401 for a detailed analysis of the force model used, and of how it is implemented in the dynamical matrix is given.

[46] Note that in order to properly estimate the interlayer force-constant parameters, an inspection of the eigenvectors of the Dirac modes in the *AA* structure, besides their energies, is needed.

[47] P. Giannozzi, S. Baroni, N. Bonini, M. Calandra, R. Car, C. Cavazzoni, D. Ceresoli, G. L. Chiarotti, M. Cococcioni, I. Dabo, A. D. Corso, S. de Gironcoli, S. Fabris, G. Fratesi, R. Gebauer, U. Gerstmann, C. Gougoussis, A. Kokalj, M. Lazzeri, L. Martin-Samos *et al.*, J. Phys.: Condens. Matter **21**, 395502 (2009).

[48] P. Giannozzi Jr, O. Andreussi, T. Brumme, O. Bunau, M. B. Nardelli, M. Calandra, R. Car, C. Cavazzoni, D. Ceresoli, M. Cococcioni, N. Colonna, I. Carnimeo, A. D. Corso, S. de Gironcoli, P. Delugas, R. A. DiStasio, A. Ferretti, A. Floris, G. Fratesi, G. Fugallo *et al.*, J. Phys.: Condens. Matter **29**, 465901 (2017).

[49] P. Giannozzi, O. Baseggio, P. Bonfà, D. Brunato, R. Car, I. Carnimeo, C. Cavazzoni, S. de Gironcoli, P. Delugas, F. Ferrari Ruffino, A. Ferretti, N. Marzari, I. Timrov, A. Urru, and S. Baroni, J. Chem. Phys. **152**, 154105 (2020).

[50] J. P. Perdew, K. Burke, and M. Ernzerhof, Phys. Rev. Lett. **77**, 3865 (1996).

[51] H. J. Monkhorst and J. D. Pack, Phys. Rev. B **13**, 5188 (1976).

[52] S. Grimme, J. Comput. Chem. **27**, 1787 (2006).

[53] S. Baroni, S. de Gironcoli, A. Dal Corso, and P. Giannozzi, Rev. Mod. Phys. **73**, 515 (2001).

[54] F. Guinea and N. R. Walet, Proc. Natl. Acad. Sci. **115**, 13174 (2018).

[55] F. Wu, T. Lovorn, E. Tutuc, I. Martin, and A. H. MacDonald, Phys. Rev. Lett. **122**, 086402 (2019).

[56] S. Carr, S. Fang, and E. Kaxiras, Nat. Rev. Mater. **5**, 748 (2020).

[57] Y. Zhang, T. Liu, and L. Fu, Phys. Rev. B **103**, 155142 (2021).

[58] N. R. Walet and F. Guinea, Phys. Rev. B **103**, 125427 (2021).

[59] M. Angeli and A. MacDonald, Proc. Natl. Acad. Sci. USA **118**, e2021826118 (2021).

[60] H. Wang, Y. Wang, X. Cao, M. Feng, and G. Lan, J. Raman Spectrosc. **40**, 1791 (2009).

[61] L. M. Malard, D. C. Elias, E. S. Alves, and M. A. Pimenta, Phys. Rev. Lett. **101**, 257401 (2008).

[62] P. Gava, M. Lazzeri, A. M. Saitta, and F. Mauri, Phys. Rev. B **80**, 155422 (2009).

[63] A. B. Kuzmenko, L. Benfatto, E. Cappelluti, I. Crassee, D. van der Marel, P. Blake, K. S. Novoselov, and A. K. Geim, Phys. Rev. Lett. **103**, 116804 (2009).

[64] T.-T. Tang, Y. Zhang, C.-H. Park, B. Geng, C. Girit, Z. Hao, M. Martin, A. Zettl, M. Crommie, S. Louie, S. Y.R., and F. Wang, Nat. Nanotechnol. **5**, 32 (2010).

[65] E. Cappelluti, L. Benfatto, M. Manzardo, and A. B. Kuzmenko, Phys. Rev. B **86**, 115439 (2012).

[66] A. Jorio, M. Kasperczyk, N. Clark, E. Neu, P. Maletinsky, A. Vijayaraghavan, and L. Novotny, Nano Lett. **14**, 5687 (2014).

[67] V. N. Popov, J. Raman Spectrosc. **49**, 31 (2018).

[68] A. García-Ruiz, J. J. P. Thompson, M. Mucha-Kruczyński, and V. I. Fal'ko, Phys. Rev. Lett. **125**, 197401 (2020).

[69] K. Chang, Z. Zheng, J. E. Sipe, and J. L. Cheng, Phys. Rev. B **106**, 245405 (2022).

[70] T.-F. Chung, R. He, T.-L. Wu, and Y. P. Chen, Nano Lett. **15**, 1203 (2015).